Computers and Geotechnics 44 (2012) 116–131

Contents lists available at SciVerse ScienceDirect

Computers and Geotechnics

journal homepage: www.elsevier.com/locate/compgeo

Cyclic lateral response of piles in dry sand: Finite element modeling and validation

Spyros Giannakos, Nikos Gerolymos *, George Gazetas

National Technical University, Athens, Greece

ARTICLE INFO

Article history:
Received 20 October 2011
Received in revised form 21 February 2012
Accepted 25 March 2012

Keywords:
Piles
Cyclic lateral loading
Centrifuge tests
Plastic shakedown
Inelastic pile response
Pile-to-pile interaction
Pile group efficiency
Shadow effect

ABSTRACT

The response of a vertical pile embedded in a dry dense sand when subjected to cyclic lateral loading is studied numerically. Three-dimensional finite element analyses with a new constitutive model of cyclic behavior of sand reproduce published centrifuge tests results. Three types of cyclic loading, two asymmetric and one symmetric are applied. Performance measure parameters (the normalized tangent and secant stiffnesses with respect to the first cycle of loading and the relative pile head displacement between two consecutive loading-unloading reversal points) are introduced to evaluate the results of the overall response of the pile–soil system. The results replicate the plastic shakedown response of the pile -soil system during cyclic loading, a response which is attributed to two mechanisms (a) soil densification and (b) "system" densification due to the gradual enlargement of the resisting soil mass to greater depths with cyclic loading. It is shown that the hardening mechanism of "system" densification dominates upon soil densification in cyclic loading. The response of a 1 × 2 pile group under cyclic lateral loading is also numerically investigated, emphasizing the role of cyclic loading on (a) the pile-to-pile interaction, (b) the additional pile distress due to the group effect, and (c) the shadow effect.

1. Introduction

The response of piles to lateral loading has been the subject of numerous studies in the last decades. However, only a limited amount of them address the effects of cyclic loading on pile response. Different methods of varying degree of accuracy have been used, incorporating simplified [1–3] or advanced [4–8] numerical models. Centrifuge experiments [9] and full-scale tests have also been performed on the cyclic behavior of piles embedded in sand [10–12].

One of the first thorough studies on the lateral response of cyclically loaded piles was carried out by Poulos [13]. According to this study, there are two phenomena that may contribute to the increased deflection of laterally loaded piles with increasing number of cycles:

(1) Structural "shakedown" of the pile–soil system. This phenomenon occurs on every pile embedded in an elastoplastic soil mass whose properties remain unaltered. When the accumulated permanent deformations stabilize "shakedown" will occur, otherwise, incremental collapse will result.
(2) Soil stiffness decay and strength degradation.

In general, during cyclic loading it is observed that: (i) both deflection and moment increase with increasing number of cycles and load magnitude, (ii) the ultimate lateral load capacity decreases with increasing number of cycles and load magnitude, (iii) effects of cyclic degradation are more severe for stiff than for soft soils, (iv) the main features of pile response to cyclic loading are practically unaffected by soil inhomogeneity, (v) the loading rate has a significant effect on the pile response, with the deflections at a given load decreasing as the loading rate increases, (vi) the location of the plastic hinge moves deeper when the pile is subjected to fully cyclic loading than to monotonic loading, due to soil stiffness degradation [11], (vii) one-way cyclic lateral loads induce more permanent strains and greater cumulative deformations of the piles than the two-way cyclic lateral loads [3], (viii) the effect of group action increases with increasing load. Thus at large deformations, the group capacity appears to be significantly lower than the sum of the capacities of each individual pile [10], (ix) the deflection of the piles in the group is significantly greater than that of a single pile under a load equal to the average load per pile [10] and (x) for a given displacement the leading row piles carry the largest load, while for a given load the maximum bending moment develops at the trailing row [12].

In this paper a simplified constitutive soil model for the cyclic lateral response of piles in cohesionless soil is developed. Implemented in a three dimensional finite element code, the model is applied to three centrifuge experiments on a pile in dry sand. The first test is used as benchmark for the calibration of model parameters. The model is further utilized to the analysis of a case study involving a group of 1 × 2 piles with similar characteristics to those of the centrifuge tests. Interesting conclusions are highlighted for

* Corresponding author. Tel.: +30 210 6018586; fax: +30 210 7722405.
E-mail address: gerolymos@gmail.com (N. Gerolymos).

0266-352X/$ - see front matter © 2012 Elsevier Ltd. All rights reserved.
http://dx.doi.org/10.1016/j.compgeo.2012.03.013

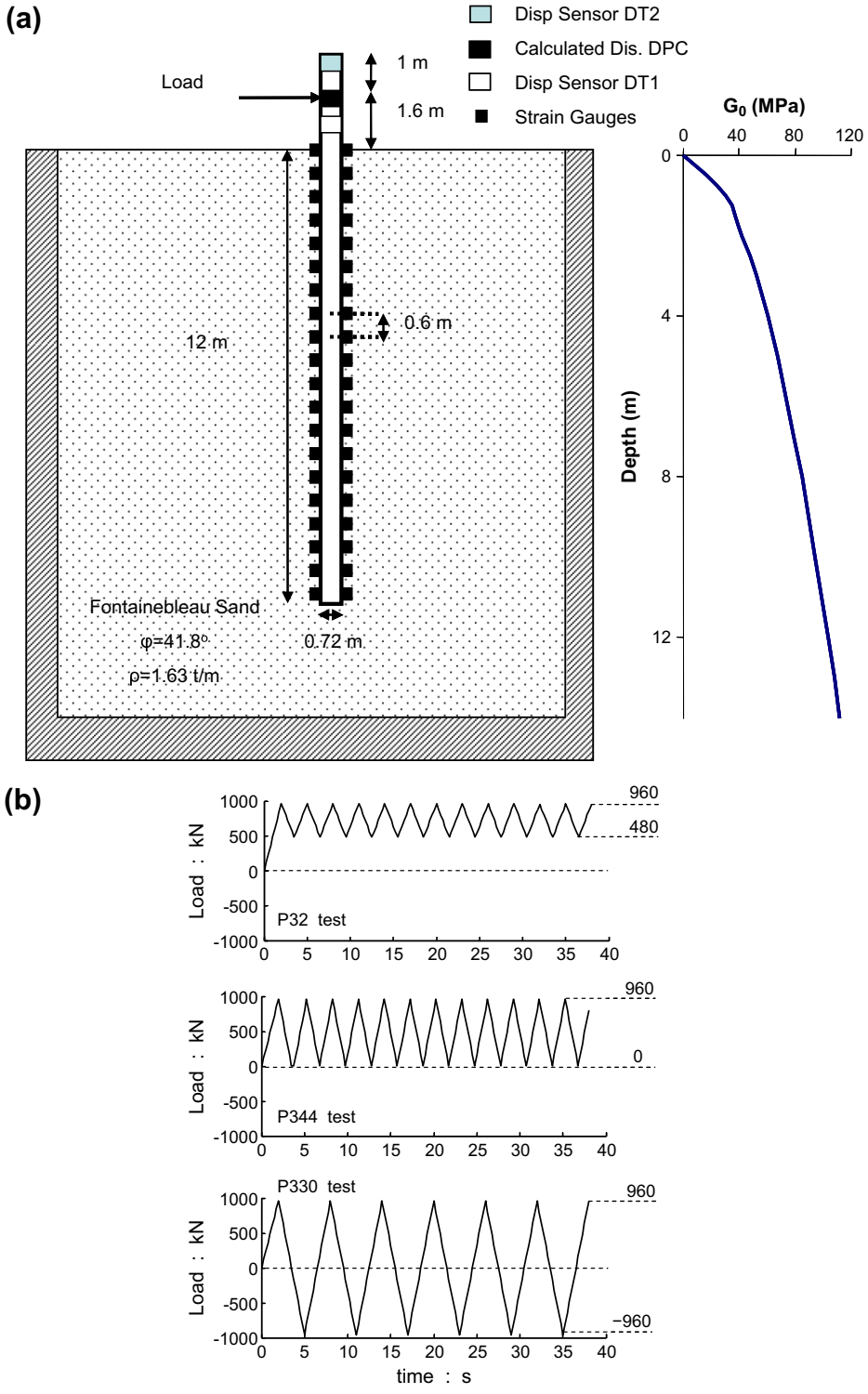

Fig. 1. (a) Experimental setup of the centrifuge tests conducted in LCPC. (b) Load time histories of the three tests (P32, P344 and P330). All dimensions refer to the modeled prototype.

the "shadow" effect on soil resistance and pile-to-pile interaction at small and large deformations.

The comparison sheds light on some complicated features of the pile response regarding (a) the observed plastic shakedown behavior, (b) the effect of the two mechanisms that result in the plastic shakedown response of the pile. That is (b1) soil densification due to voids reduction, and (b2) "system" densification due to the gradual enlargement of the resisting soil mass to greater depths with cyclic loading (c) the influence of the number of cycles on the internal structural forces (residual and maximum) and soil reactions of the pile, and (d) the efficiency of the pile group: (d1) it presents the efficiency factor as a function of the horizontal pile displacement, (d2) it bridges the gap between pile-to-pile interaction at extremely small (elastic response) and at very large (plastic response) deformations, (d3) it highlights the role of cross-coupling pile-to-pile interaction factors that are usually neglected in a pile

Table 1
Pile characteristics.

Name	Symbol	Model scale	Prototype scale (40 g)
Length	L	36.5 cm	14.6 m
Depth of pile tip from ground surface	D	30 cm	12 m
External diameter	B	1.8 cm	0.72 m
Internal diameter		1.5 cm	0.6 m
Young's modulus	E	7.4×10^4 MPa	
Moment of inertia	I	2.67×10^{-9} m^4	6.83×10^{-3} m^4
Bending stiffness	EI	197 N m^2	505 MN m^2
Elastic limit	σ_e	245 MPa	

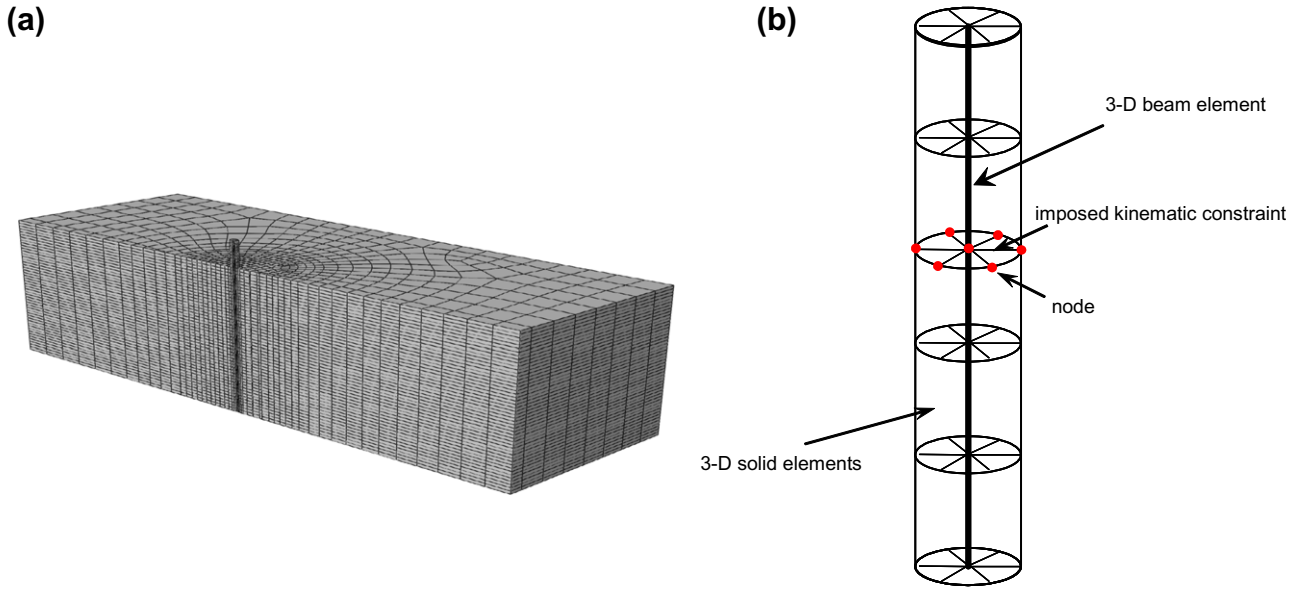

Fig. 2. (a) Finite element modeling of the centrifuge test. (b) Pile modeling.

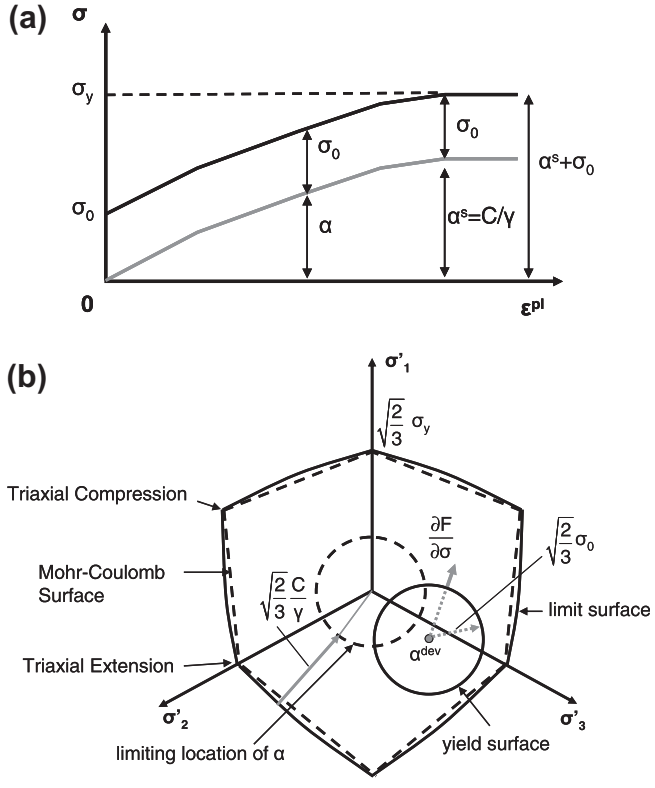

Fig. 3. (a) Simplified one-dimensional representation of the hardening of the proposed constitutive model. (b) Three-dimensional representation of the hardening in the nonlinear kinematic model.

group response analysis. Finally, appropriately defined performance measure parameters are introduced to evaluate the pile response and to unravel the contribution of soil and "system" densification to the plastic shakedown mechanism.

2. Centrifuge lateral cyclic load pile experiments

Three centrifuge tests on a single pile subjected to cyclic horizontal loading were performed by Rosquoët et al. [14] at Laboratoire Central des Ponts et Chaussées (LCPC). The centrifuge

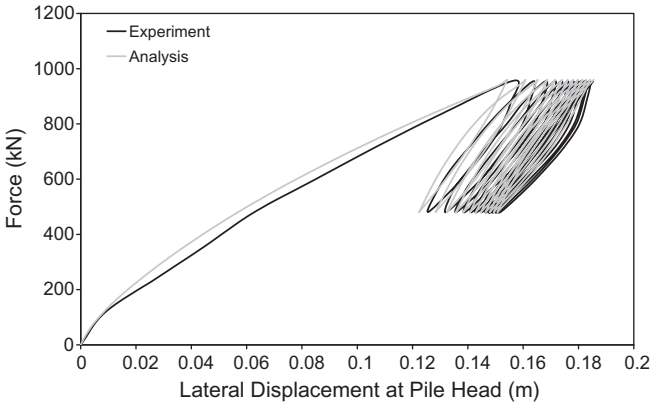

Fig. 4. Experimental and computed force–displacement curves at pile head for test P32.

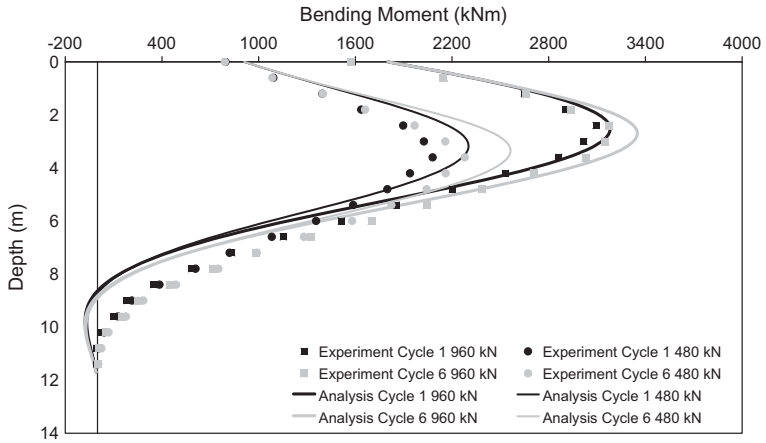

Fig. 5. Comparison of computed and recorded bending moment distributions for test P32 at two different stages of loading: at 1st and 6th cycles. The maximum applied load is 960 kN and the minimum 480 kN.

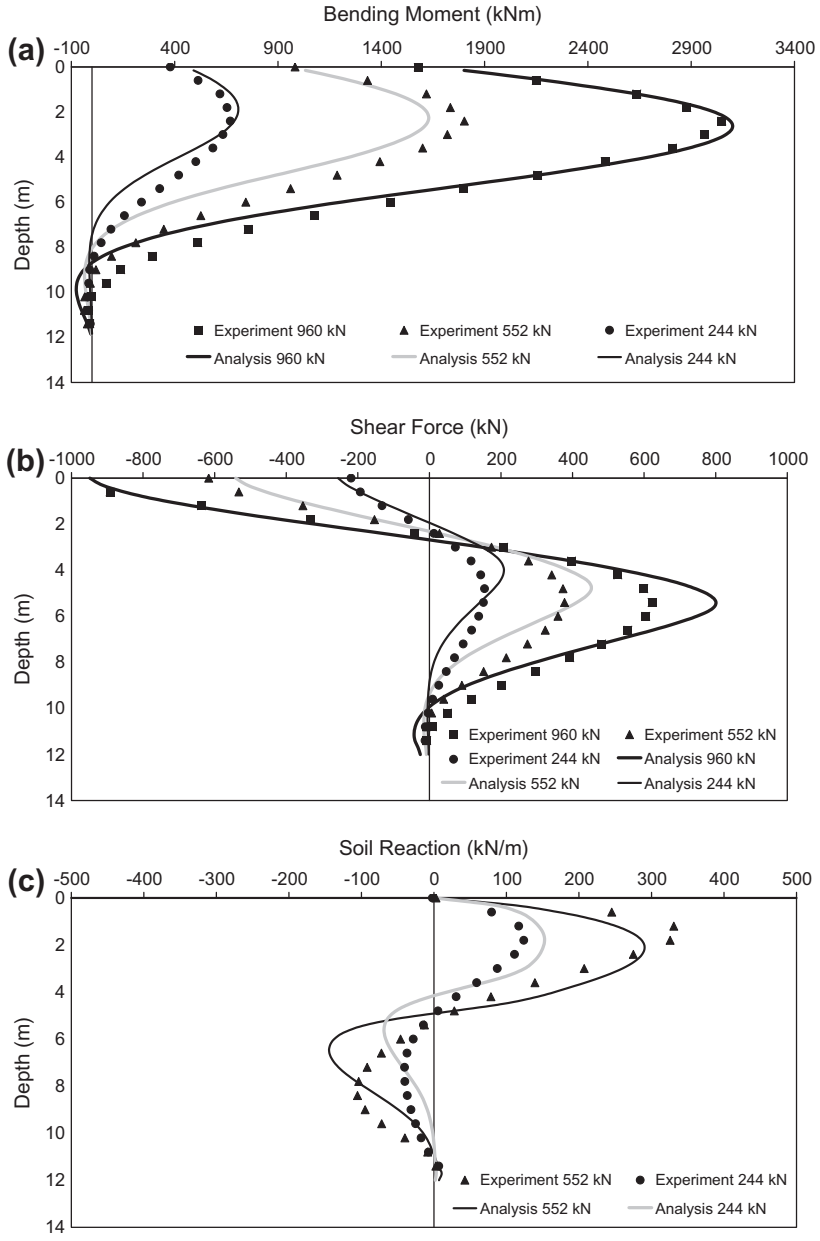

Fig. 6. Comparison of computed and recorded (a) bending moment, (b) shear force and (c) soil reaction distributions for virgin loading of test P32 at 960 kN, 552 kN and 244 kN.

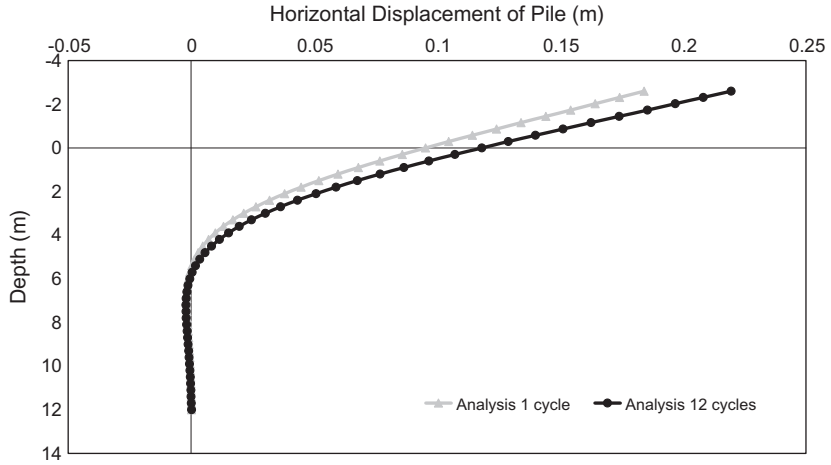

Fig. 7. Comparison of computed horizontal displacement of the pile for test at two different stages of loading: at the end of the 1st and 12th cycles. The maximum applied load is 960 kN.

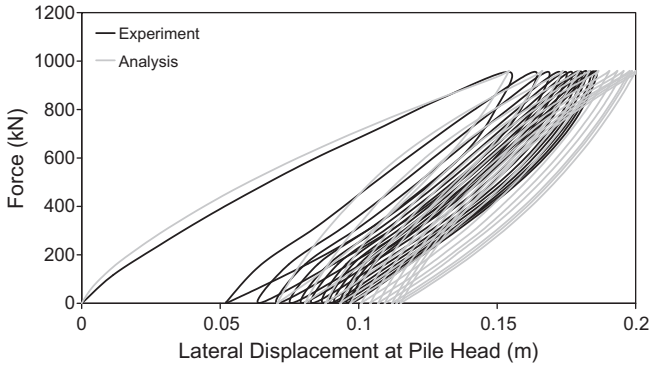

Fig. 8. Experimental and computed force–displacement curves at pile head for test P344.

models were 1/40 in scale and involved pile head loading with three different force time histories. The loading time histories were: (i) 12 cycles from 960 kN to 480 kN (test P32) (ii) 12 cycles from 960 kN to 0 kN (test P344) (iii) 6 cycles from 960 kN to −960 kN (test P330). The experimental set up and the loading time histories in prototype scale are portrayed in Fig. 1.

The cyclic lateral load tests were conducted on a vertical friction pile placed in a sand mass of uniform density. The Fontainebleau sand centrifuge specimens were prepared by the air sand-raining process into a rectangular container (80 cm wide by 120 cm long by 36 cm deep), with the use of a special automatic hopper developed at LCPC [15]. The unit weight and the relative density of the specimen were measured to be $\gamma_d = 16.5 \pm 0.04\ \mathrm{kN/m^3}$ and $D_r = 86\%$, respectively. Laboratory results from drained and undrained torsional and direct shear tests on Fontainebleau sand reconstituted specimens indicated mean values of peak and critical-state angles of $\varphi_p = 41.8°$ and $\varphi_{cv} = 33°$, respectively.

The model pile is a hollow aluminum cylinder of 18 mm external diameter, 3 mm wall thickness, and 365 mm length. The flexural stiffness of the pile is $0.197\ \mathrm{kN\,m^2}$ and the elastic limit stress of the aluminum is 245 MPa. The centrifuge tests were carried out at 40 g and the characteristics of the model and the prototype pile are presented in Table 1.

The instrumentation included two displacement sensors, located at the section of the pile above the ground surface, and 20 pairs of strain gauges, positioned along the length of the pile so that the bending moment profile $M(z)$ could be measured during the tests. The resultant earth pressure $p = p(z)$, per unit length along the pile, was obtained by double differentiation of $M(z)$ as

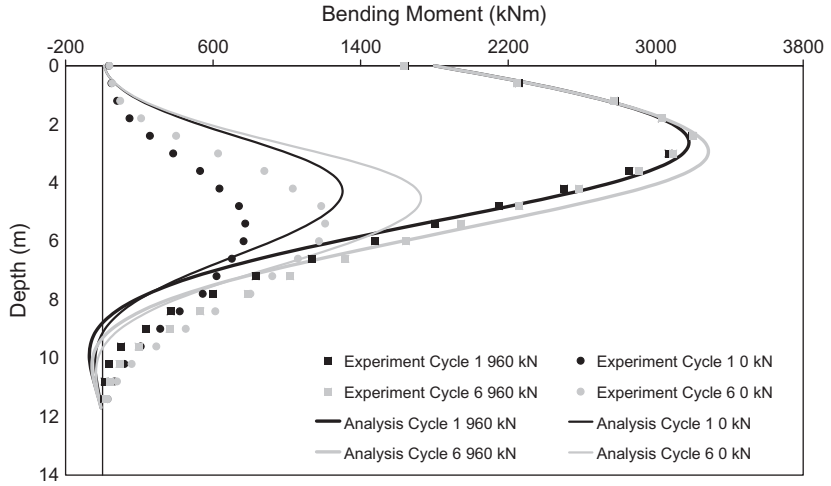

Fig. 9. Comparison of computed and recorded bending moment distributions for test P344 at two different stages of loading: at the 1st and 6th cycles. The maximum applied load is 960 kN and the minimum 0 kN.

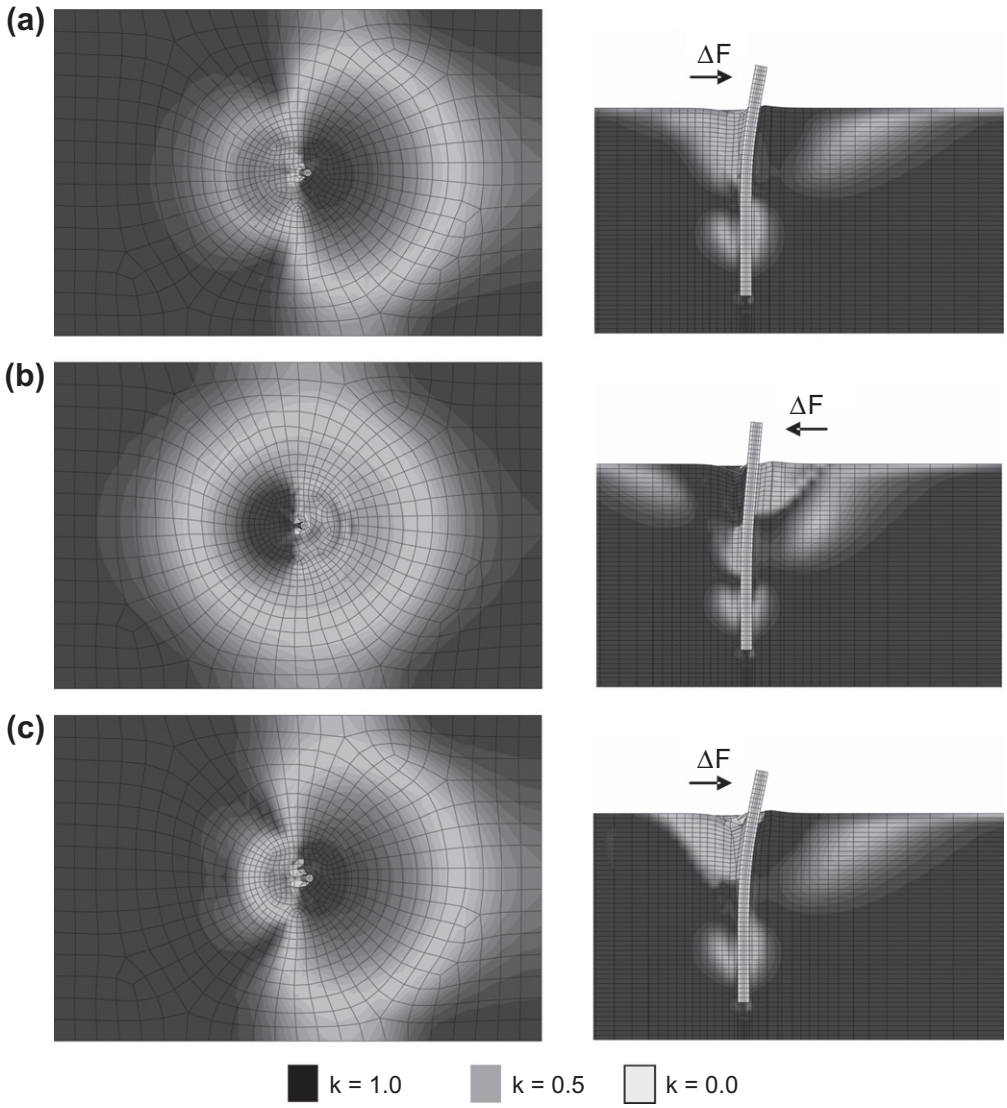

Fig. 10. Contours of the active and passive stress states in terms of the state parameter k at three different stages of loading of the single pile: (a) at the 1st cycle at 960 kN, (b) at the 12th cycle at 0 kN, and (c) at the 12th cycle at 960 kN. $k = 1$ corresponds to pure triaxial compression loading condition (passive state), and $k = 0$ to pure triaxial extension loading condition (active state) while $k \approx 0.5$ sets the boundaries between the active and the passive state. (Deformation scale factor = 5.)

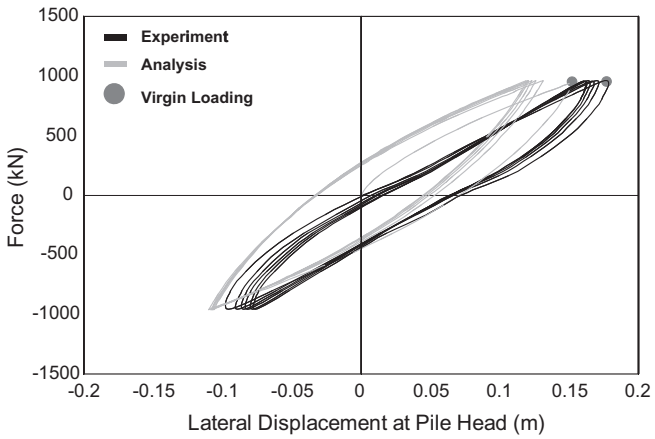

Fig. 11. Experimental and computed force–displacement curves at pile head for test P330.

proposed in Reese and Van Impe (see for instance [16]) using high-order spline interpolation and assuming hinged boundary conditions at the pile tip [17]. The strain gauges were spaced at 0.6 m in prototype scale starting from the ground level to the pile tip. This single pile was driven into the sand at 1 g before rotating of the centrifuge. In flight, the single pile was subjected quasi-statically to horizontal cyclic loading through a servo-jack connected to the pile with a cable. With such a configuration the pile head is not submitted to any parasitic bending moment. The results for the three cyclic loading tests were obtained in the form of horizontal force–displacement time histories at the head of the pile, as well as of bending moment along the pile.

3. Finite element modeling

The above mentioned centrifuge tests were modeled numerically in 3D using the finite element code ABAQUS. The pile is assumed to be linear elastic while the cyclic soil behavior is described via a nonlinear constitutive law with kinematic hardening law and associated plastic flow rule. Fig. 2 depicts the finite element discretization for the centrifuge tests. The distance from the pile tip to the bottom of the boundaries is 2.4 m (3.3 pile

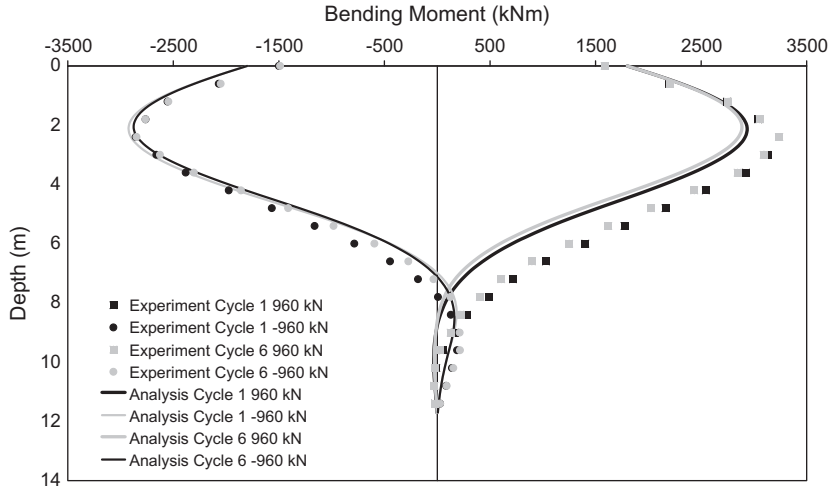

Fig. 12. Comparison of computed and recorded bending moment distributions for test P330 at the end of the 1st and 6th cycle of loading (positive values of bending moment) and unloading (negative values of bending moment), respectively.

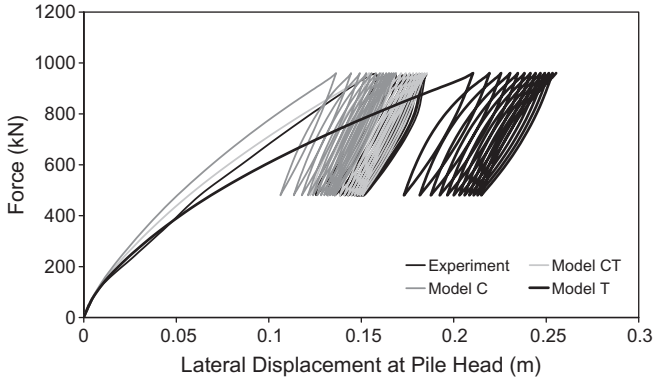

Fig. 13. Force–displacement curves at pile head for test P32 computed by the three constitutive soil models.

diameters). Approximately 43,000 elements were used for each analysis. The soil is modeled with 8-node brick elements while the pile is replaced by 3D beam elements placed at its center and connected with appropriate kinematic constraints with the nodes at the perimeter of the pile, in order to model the complete geometry of the pile. The solid elements inside the perimeter of the pile have no stiffness. In this way, each pile section behaves as a rigid disk: rotation is allowed on the condition that the disk remains always perpendicular to the beam axis, but stretching cannot occur.

The element size is small enough (0.3 m in the vertical direction) (a) to capture intense plastic strain concentration at the pile–soil interfaces, (b) to capture more accurately the pile-to-pile interplay in case of a pile group, and (c) to include the vertical position of the strain gauges along the pile in order to achieve a direct comparison with the measurements. The mesh is refined up to a distance of seven diameters around the pile in order to acquire an accurate distribution of soil yielding. When the cohesionless soil reaches the active state as the pile is laterally loaded, it collapses and flows with the pile. Thus, no gap is formed and no interface elements are used in the analysis. Furthermore, the change of the stress in the soil during the pile installation is very small compared to the stress variation in soil due to lateral loading of the pile and for this reason the effects of pile installation are omitted [6]. Finally, the bottom and side boundaries were fixed in order to model the box of the centrifuge tests.

4. Constitutive soil model

The plasticity model used in this study for cohesionless soil is an extension of the model used by Gerolymos et al. [18,19] for cohesive soils. Soil behavior is modeled through a constitutive model with kinematic hardening and associated plastic flow rule. According to this model, the evolution of stresses is described by the relation:

$$\sigma = \sigma_0 + \alpha \tag{1}$$

where σ_0 is the value of stress at zero plastic strain, assumed to remain constant. The parameter α is the "backstress", which defines the kinematic evolution of the yield surface in the stress space. Integration of the backstress evolution law over a half cycle of a unidirectional load (e.g. tension or compression) yields the following expression:

$$\alpha = \frac{C}{\gamma}[1 - \exp(-\gamma\varepsilon^{pl})] \tag{2}$$

in which C and γ are hardening parameters that define the maximum transition of the yield surface, and the rate of transition, respectively, and ε^{pl} is the plastic strain. Differentiating α with respect to ε^{pl} and taking the limit at zero, one obtains for parameter C:

$$\left.\frac{\partial\alpha}{\partial\varepsilon^{pl}}\right|_{\varepsilon^{pl}\to 0} = C = E \tag{3}$$

where E is the modulus of elasticity.

The evolution law of the model consists of two components: a kinematic hardening component, which describes the translation of the yield surface in the stress space (defined through the backstress α), and an isotropic hardening component, which defines the size of the yield surface σ_0 at zero plastic deformation. The kinematic hardening component is defined as an additive combination of a purely kinematic term (linear Ziegler hardening law) and a relaxation term (the recall term), which introduces the nonlinearity. The evolution of the kinematic component of the yield stress is described as follows:

$$\dot{\alpha} = C\frac{1}{\sigma_0}(\sigma - \alpha)\dot{\varepsilon}^{pl} - \gamma\alpha\dot{\varepsilon}^{pl} \tag{4}$$

where $\dot{\varepsilon}^{pl}$ is the plastic flow rate (obtained through the equivalent plastic work), $\dot{\varepsilon}^{pl}$ the equivalent plastic strain rate:

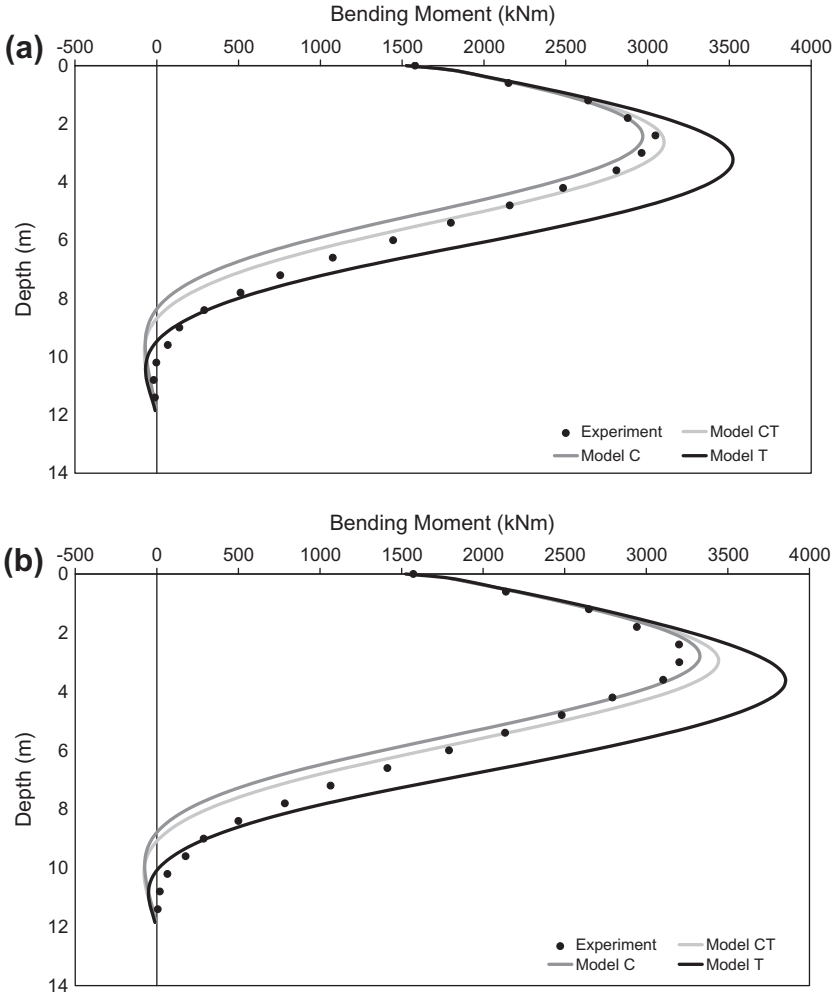

Fig. 14. Comparison of computed (solid lines) with the three constitutive soil models and recorded (circles) bending moment distributions for test P32, at two different stages of loading: at the end of the 1st and 12th cycles. The maximum applied load is 960 kN.

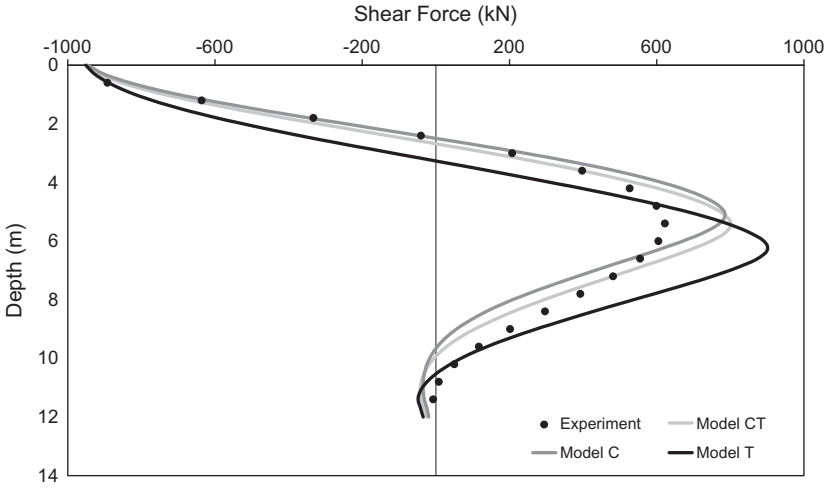

Fig. 15. Comparison of computed (solid lines) with the three constitutive soil models and recorded (circles) shear force distributions for test P32, at the end of the first cycle. The maximum applied load is 960 kN.

$$\dot{\bar{\varepsilon}}^{pl} = \sqrt{\frac{2}{3}\dot{\varepsilon}^{pl} : \dot{\varepsilon}^{pl}} \tag{5}$$

The evolution law for the kinematic hardening component implies that the backstress is contained within a cylinder of radius:

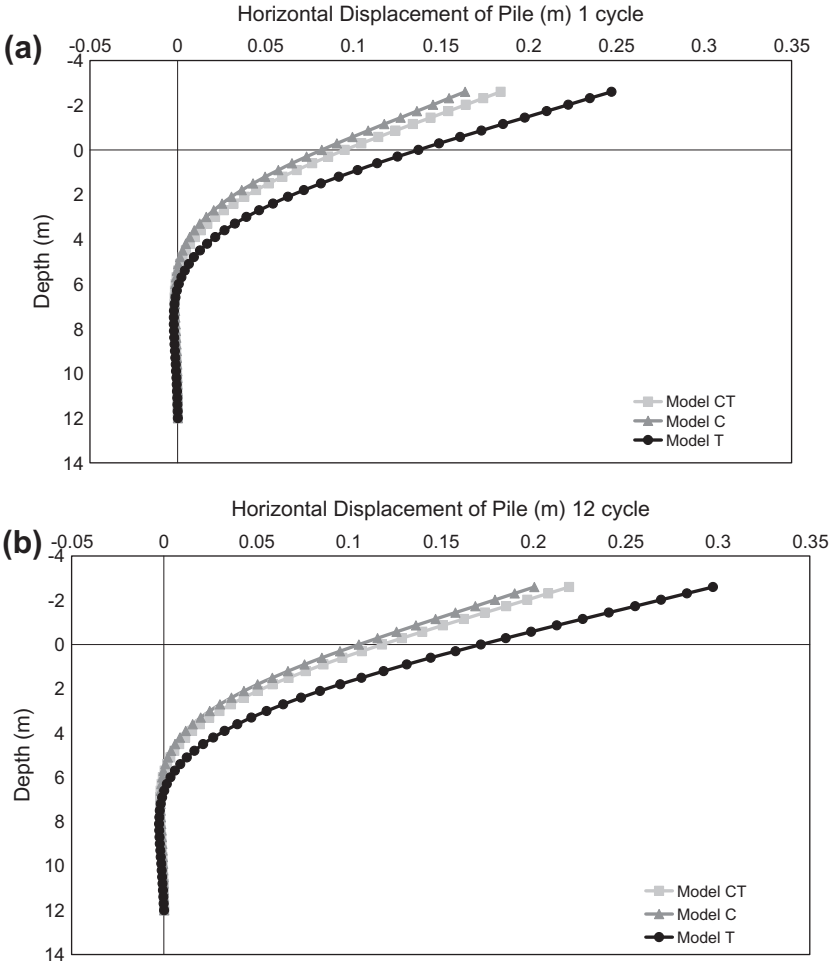

Fig. 16. Comparison of horizontal displacement distributions for test P32, computed with the three constitutive soil models, at different stages of loading: at the end of the 1st and 12th cycles. The maximum applied load is 960 kN.

$$\sqrt{\frac{2}{3}}\alpha_s = \sqrt{\frac{2}{3}}\frac{C}{\gamma} \tag{6}$$

where α_s is the magnitude of α at saturation. Since the yield surface remains bounded, this implies that any stress point must lie within a cylinder of radius $\sqrt{(2/3)}\sigma_y$. At large plastic strains, any stress point is contained within a cylinder of radius $\sqrt{(2/3)}\,(\alpha_s + \sigma_s)$ where σ_s is the equivalent stress defining the size of the yield surface at large plastic strain, and σ_y is the uniaxial yield stress given by:

$$\sigma_y = \frac{C}{\gamma} + \sigma_0 \tag{7}$$

In the Mohr–Coulomb failure criterion σ_y is equal to:

$$\sigma_y = \sqrt{3J_2} \tag{8}$$

in which $\sqrt{J_2}$ is the square root of the second deviatoric stress invariant that satisfies the following equation:

$$I_1 \sin\varphi + \frac{1}{2}\left[3(1-\sin\varphi)\sin\theta + \sqrt{3}(3+\sin\varphi)\cos\theta\right]\sqrt{J_2} - 3c \times \cos\varphi = 0 \tag{9}$$

where I_1 is the first principal stress invariant, c, cohesion, φ, friction angle and θ the Lode angle [20] which is given by:

$$\cos(3\theta) = \frac{3\sqrt{3}}{2}\frac{J_3}{J_2^{3/2}} \tag{10}$$

where J_2 and J_3 are the second and third deviatoric stress invariants. Combining Eqs. (3) and (9) with (10) one obtains for γ:

$$\gamma = \frac{E}{\sqrt{3J_2} - \sigma_0} \tag{11}$$

A user subroutine is imported in ABAQUS, which relates the model parameters to the principal stresses and the Lode angle at every loading step. Incorporating the Lode angle effect allows for significant accuracy in three-dimensional shear response environments [21]. The yield surface of the proposed constitutive model is determined to fit the Mohr–Coulomb failure response in a triaxial loading test for both compression and extension conditions assuming linear interpolation for the intermediate stress states. For this reason, the parameter k is introduced which is a function of Lode angle and takes values from 0 to 1. $k = 0$ corresponds to pure triaxial extension conditions and $k = 1$ to pure triaxial compression conditions. In summary, the constitutive model parameters are calibrated to match the Coulomb failure criterion on the principal stresses plane for every apex of the hexagon with the smooth envelope of Fig. 3.

The distribution of Young's Modulus varies parabolically with depth according to:

$$C = E = E_0\left(\frac{\sigma_v}{P_a}\right)^m \tag{12}$$

where E_0 is the reference Young's Modulus, σ_v the vertical stress, P_a the atmospheric pressure (approximately 100 kPa) and m a parameter that defines the rate of increase of E with depth.

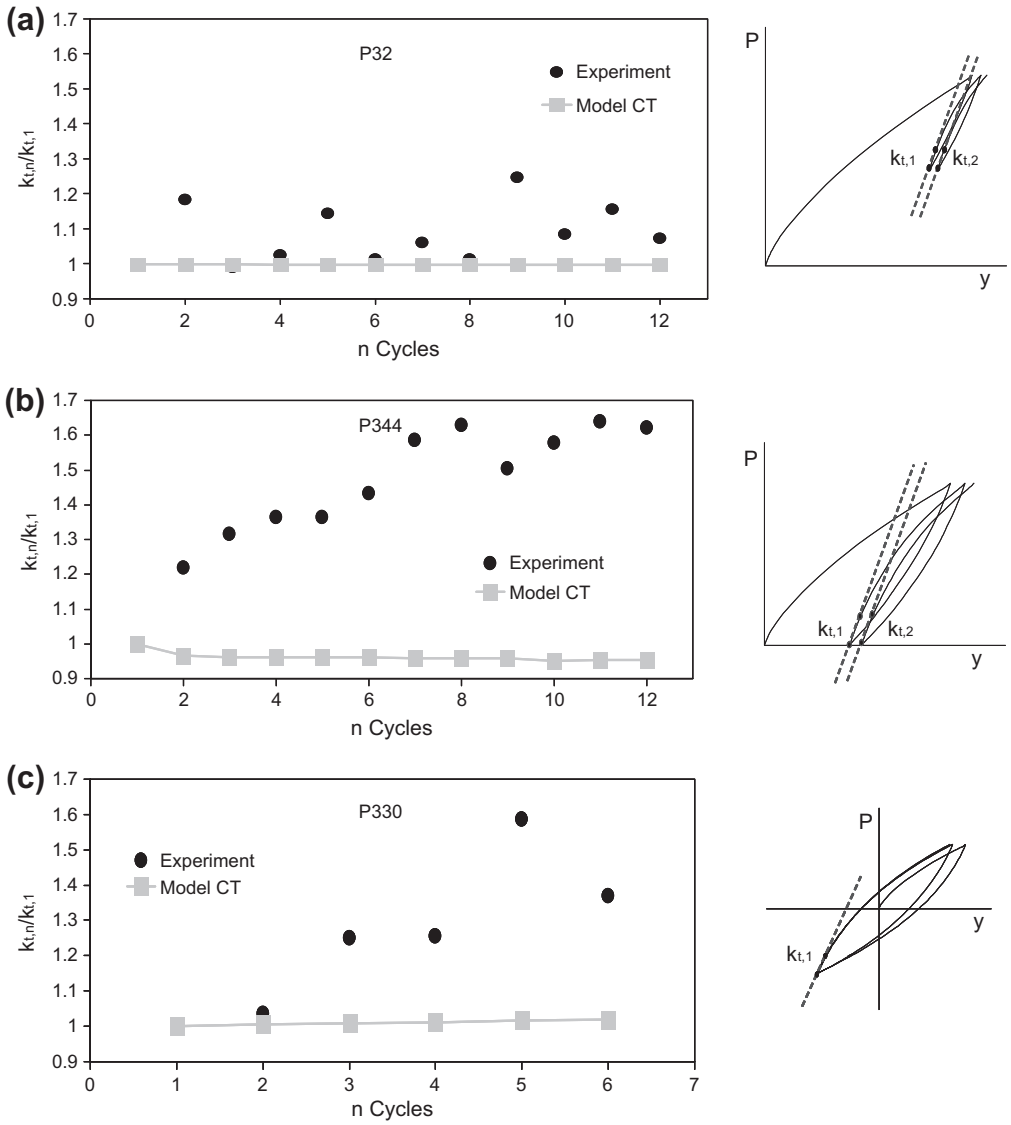

Fig. 17. Normalized tangent stiffness with respect to the first cycle of loading, for: (a) test P32, (b) test P344, and (c) test P330.

Obviously, the model in its present form cannot reproduce either dilative response or volume contraction (soil densification) with cyclic loading. Since soil volume reduction dominates the response in a loading with a large number of cycles, the role of the first weakness is usually of insignificant importance. The second drawback of the proposed model will be efficiently used in the sequel as a reference point for evaluating the role of the two hardening mechanisms ("system" and soil densification) responsible for the observed plastic shakedown response of the pile.

5. Numerical simulation of the centrifuge tests

The model is first calibrated against the one-way cyclic loading test with maximum horizontal force 960 kN and minimum horizontal force 480 kN (test P32). Subsequently, it is applied to predict the measured data of the other two tests (P330 and P344). The three tests differ by the characteristics of the cyclic loading sequences since one-way and two-way loading at different load amplitudes are used. It should be noted that the applied loads always stay in the domain of service loads.

5.1. Calibration of model parameters against test P32

The model parameters C (E_0 = 192 MPa), m (=0.5), and γ (which is a function of the critical state friction angle φ_{cv} = 33°), were calibrated to match the experimental "force–displacement" loop at the head of the pile (Fig. 4). In this figure it is observed that the model is capable of predicting the plastic shakedown response of the pile. This response is the resultant of the following two mechanisms: (a) Soil densification due to the reduction of voids, and (b) "System" densification due to the gradual enlargement of the resisting soil mass to greater depths with cyclic loading. Only the second mechanism is captured by the proposed model.

Fig. 5 compares the bending moment profiles at the 1st and 6th cycles of loading. In general, the agreement between the measured and the computed curves is quite satisfactory. The model predicts well the shape of the moment distribution and the increase of the bending moments with increasing number of cycles. The model is also capable of predicting the depth of the maximum bending moment both for loading and unloading conditions as well as the shift of the maximum bending moment at a higher depth as the number of cycles increases.

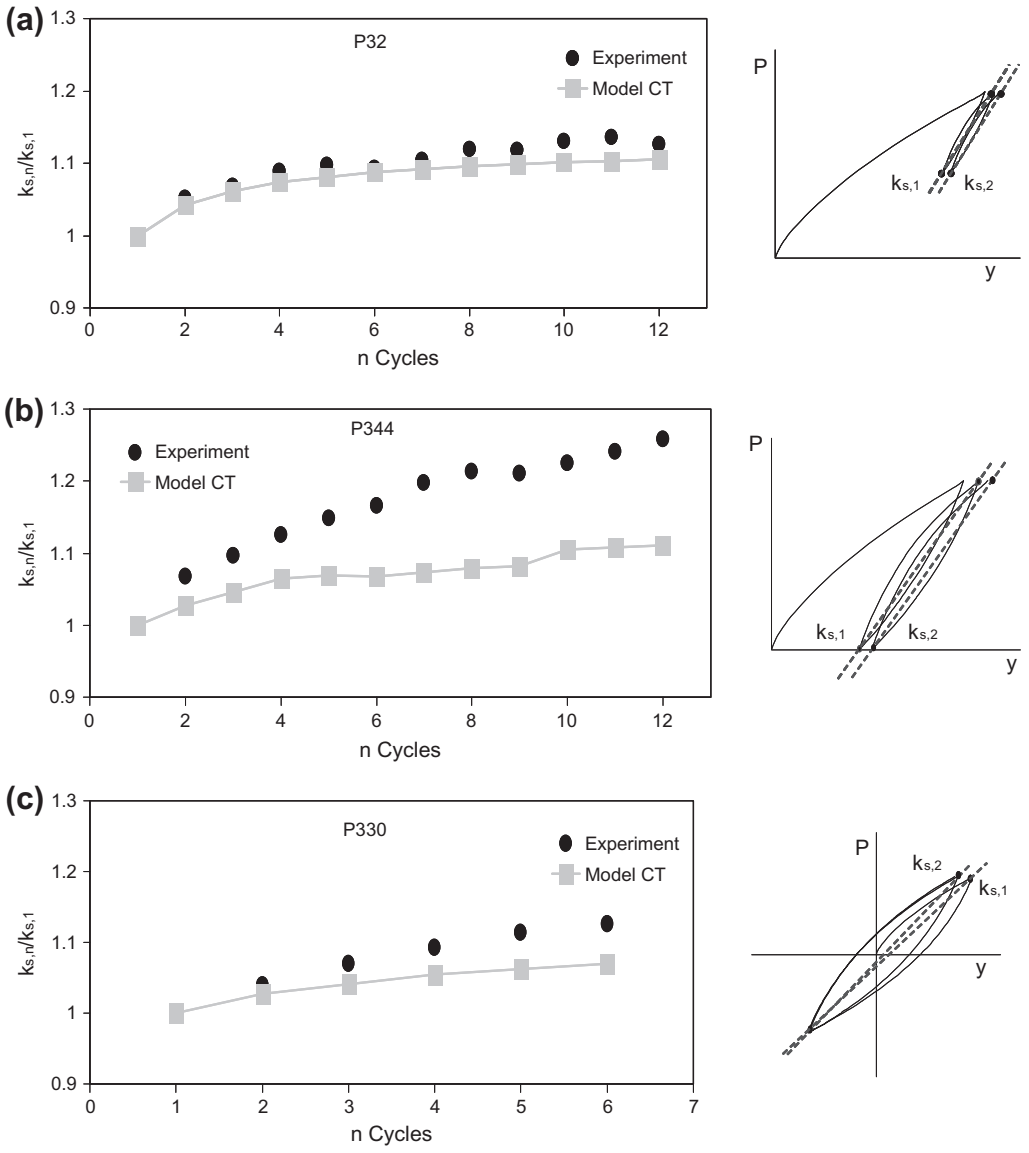

Fig. 18. Normalized secant horizontal pile stiffness with respect to the first cycle of loading, for: (a) test P32, (b) test P344, and (c) test P330.

Because shear force and soil reaction were calculated indirectly from the measured bending moment during the experiment, a comparison with the calculated bending moment shear force and soil reaction (Fig. 6) at different stages of virgin loading is presented. In general, the agreement between measured and computed curves is quite satisfactory. Some differences are noted in the soil reaction curves which can be partly attributed to errors in the spline interpolation process. But even in this case, the model captures the increase in both (a) the magnitude of the maximum soil reaction, and (b) the depth at which this maximum occurs.

Fig. 7 shows comparison between the displacement profiles at the end of the 1st and 12th cycles. The difference is attributed to the accumulation of soil plastification with number of cycles. It should be noted that the displacement profiles have a nearly triangular shape, vanishing at $z = 6$ m, implying that the effective length of the pile is only a 50% of its total length.

5.2. Comparison of numerical results with tests P344 (symmetric cyclic loading) and P330 (asymmetric cyclic loading)

The calibrated model (from the P32 test) is utilized to predict the results of the P344 test (cyclic loading without sign reversal) and the P330 test (fully cyclic loading with sign reversal).

Test P344 is a full one-way cyclic loading test with maximum horizontal force 960 kN and minimum horizontal force 0 kN. The computed force–displacement curve at the pile head is compared to the experimental data in Fig. 8. Despite the discrepancy in the residual displacement at the pivot point of each unloading phase, the comparison is quite satisfactory. Fig. 9 shows the comparison between measured and computed bending moment profiles. The discrepancy in the unloading phase is attributed to the developed soil constitutive model not reproducing soil densification.

Finally, Fig. 10 depicts the contours of the active and passive stress states in terms of the state parameter k at three different stages of: (a) at the 1st cycle at 960 kN, (b) at the 12th cycle at

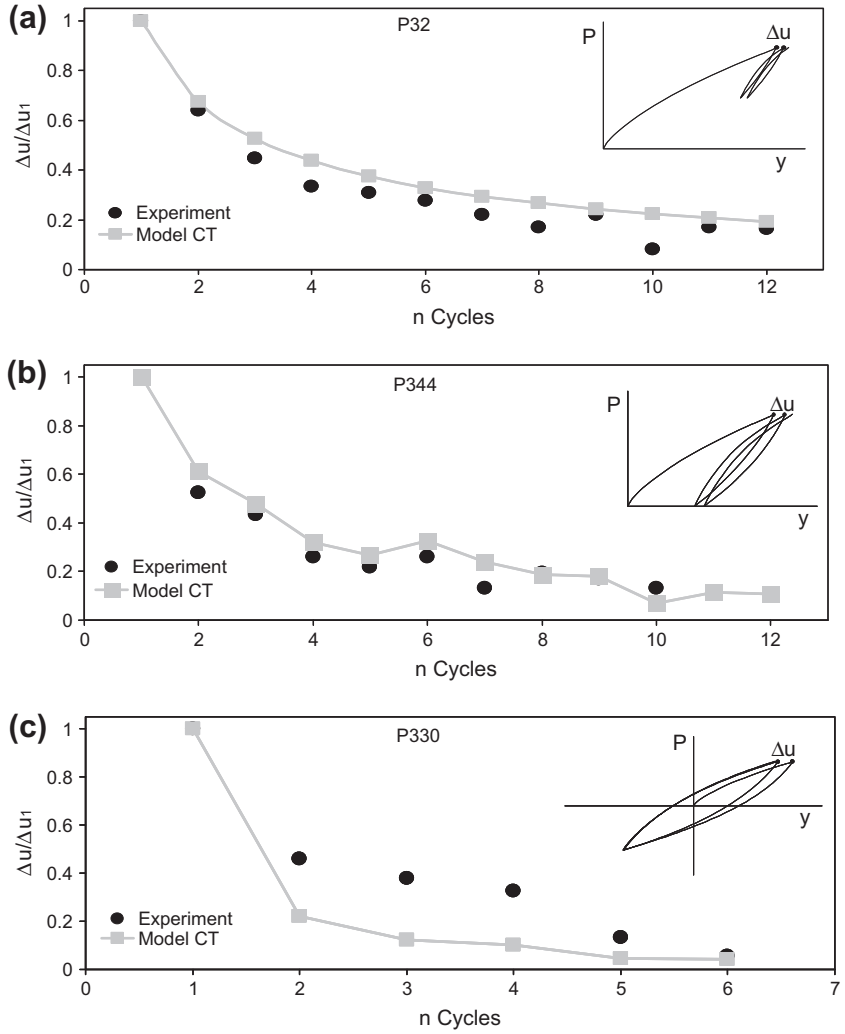

Fig. 19. Relative pile head displacement between two consecutive re-loading–unloading reversal points normalized with the one between the virgin loading–unloading and the first re-loading–unloading reversal points, for: (a) test P32, (b) test P344, and (c) test P330.

0 kN, and (c) at the 12th cycle at 960 kN. $k = 1$ corresponds to pure triaxial compression loading condition (passive state), and $k = 0$ to pure triaxial extension loading condition (active state) while $k \approx 0.5$ sets the boundaries between the active and the passive state.

It is interesting to observe that the plastic shakedown effect is reflected by the gradually developing fan-shaped stress bulb, the frontal part of which represents the mobilized soil mass that is in a passive state and expands with increasing cycles of loading, while the trailing part corresponds to the mobilized soil zone that is in an active state and shrinks with increasing number of cycles. The larger the bulb of "passive" stresses the greater the lateral soil reactions that resist the applied load, and finally, the pile reaches a steady state equilibrium of constant plastic strain (plastic shakedown).

Test P330 is a two-way cyclic loading test with maximum horizontal force 960 kN and minimum horizontal force −960 kN. The computed force–displacement curve at the pile head is compared to the experimental data (Fig. 11) for the first 6 cycles of loading. It is observed that the pile displacement at reversal decreases at a decreasing rate as the number of loading cycles increases, in contrast to the previous experiments. This hardening behavior in the pile response is attributed to the extensive soil plastification that takes place around the pile, which leads to an increase of the soil pressure on the pile. In addition, a discrepancy in the displacement of about 1.5 cm is observed at the end of the virgin loading among test P330 and tests P32 and P344. This means that the sand in this experiment was not at the same initial condition as it was in tests P32 and P344. The results in this case are more qualitative than

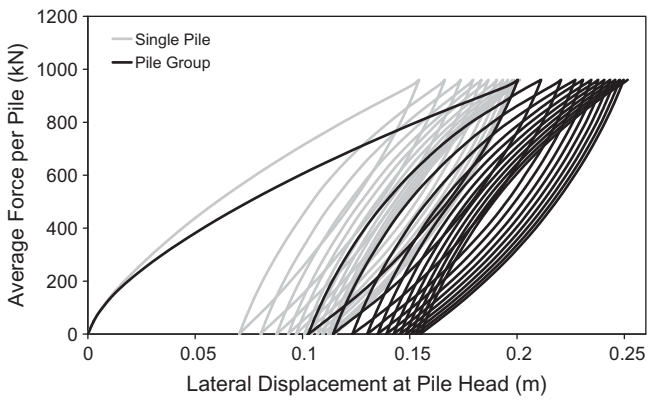

Fig. 20. Force–displacement curves of the single pile and the pile group for the loading of test P344.

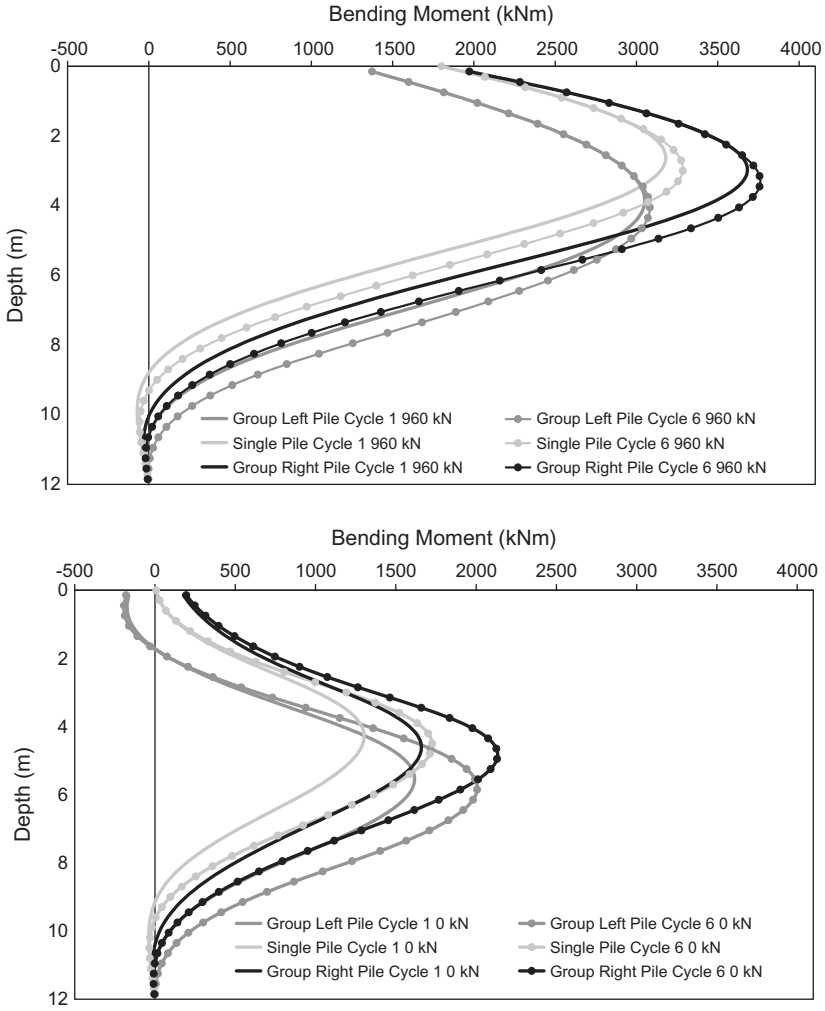

Fig. 21. Comparison of computed bending moment distributions of the pile group and the single pile for test P344 at two different stages of loading: (atop) at the 1st and 6th cycles and at 960 kN, and (bottom) at the 1st and 6th cycles and at 0 kN. The maximum applied load is 960 kN and the minimum applied one is 0 kN.

quantitative since no calibration of the proposed model was performed for the new soil condition. Fig. 12 depicts bending moment profiles at the 1st and 6th cycles of loading. For full cyclic lateral loading, the computed values of bending moment agree well with the experimental ones.

5.3. Influence of the π-plane shape of the yield surface on pile response

On the loading side of the pile where compression prevails the soil is in the passive state, while at the back of the pile, where extension dominates the response, the soil is in the active state. For this reason, the predictions of the developed constitutive model (hereafter designated as model CT) are compared with those from matching the Mohr–Coulomb yield criterion on its π-plane with a circle, in two different ways. In the first case (Model C), the circle circumscribes the Mohr–Coulomb shaped hexagonal pyramid (compressive meridian matching), while in the second case (Model T), the hexagonal pyramid is inscribed by the circle (tensile meridian matching). Due to lack of space, only the results for test P32 are presented herein.

The predictions of the three models are shown comparatively in Fig. 13. Obviously, Model CT provides the best response. Model C is close to the experimental values but with stiffer response, while Model T leads to a "softer" response. The bending moment profiles at the 1st and 12th cycles of loading are compared in Fig. 14. It is observed that Model CT captures well the bending moment distribution while the response of triaxial compression model (Model C) prediction is also close to the measured values, since the passive soil resistance is an order of magnitude greater than the active one. As expected, the triaxial extension model (Model T) overestimates the response. Fig. 15 presents the shear force profiles at the end of the first cycle. The proposed model (Model CT) captures better the shear force distribution in comparison to the triaxial compression model. Finally, Fig. 16 depicts the horizontal displacement profiles at two different levels of cyclic loading, computed from the three models. As expected, the triaxial compression model has a stiffer response than the proposed model, while the triaxial extension model predicts larger displacements and larger effective pile lengths.

5.4. Evaluation of model predictions

Three performance measure parameters are introduced to evaluate the response of the pile–soil system. Fig. 17 depicts the tangent stiffness at each unloading–reloading reversal point divided by the tangent stiffness at unloading–reloading reversal point of the first cycle, which is indicative of the elastic response of the pile. It is interesting to observe that the computed tangent stiffness remains constant for the proposed model described above, unaffected by cyclic loading, while the measured tangent

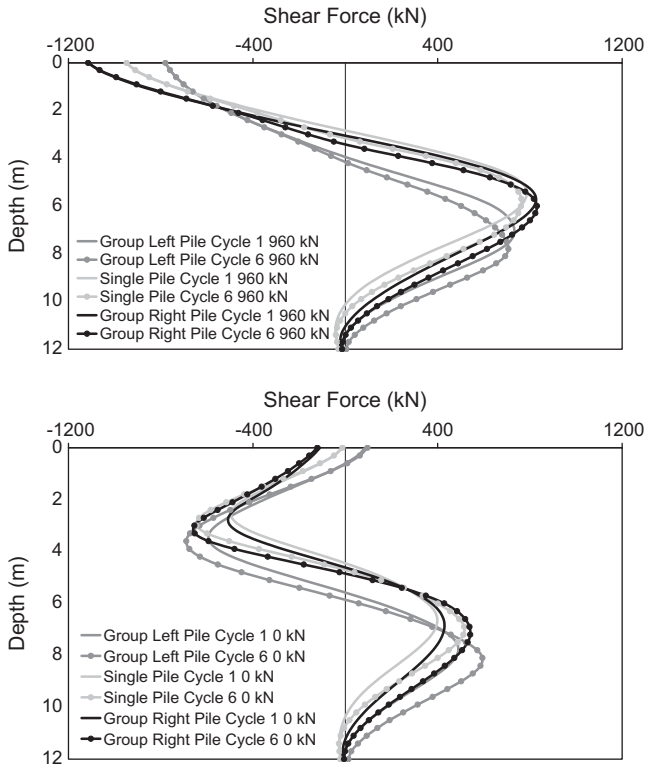

Fig. 22. Comparison of computed shear force distributions of the pile group and the single pile for test P344 at two different stages of loading: (atop) at the 1st and 6th cycles and at 960 kN, and (bottom) at the 1st and 6th cycles and at 0 kN. The maximum applied load is 960 kN and the minimum applied one is 0 kN.

stiffness increases in tests P344 and P330. This increase in the measured tangent stiffness is attributed to soil (material) densification during cyclic loading, an effect that is not simulated by the utilized soil constitutive model and which prevails in the elastic response of the pile. In test P32 the measured tangent stiffness shows a small variation without exhibiting a clear trend of hardening response, remaining practically unaffected by cyclic loading, the amplitude of which is too small to trigger soil densification.

Fig. 18 presents the secant stiffness between two sequential reversal points normalized by the secant stiffness of the first cycle, which is indicative of the overall response of the pile during cyclic loading. It is worthy of note that both the computed and the measured secant stiffnesses increase with the number of cycles. Given that the system densification is captured numerically, the difference between measured and computed response is only attributed to soil densification.

Fig. 19 presents the relative pile head displacement between two consecutive re-loading–unloading reversal points normalized with the one between the virgin loading–unloading and the first re-loading–unloading reversal points. The pile displacement at pivot points increases in the asymmetric cyclic loading or decreases in the symmetric two-way cyclic loading with a decreasing rate and the pile finally reaches a zero-plastic strain rate equilibrium. It is observed that the computed versus measured response is in well agreement, implying that the mechanism of "system" densification dominates upon that of soil densification.

6. Application to the analysis of a 1 × 2 pile group

The capability of the developed constitutive model for lateral response of piles in sand is further investigated through analysis of a 1 × 2 pile group. The piles, located at a distance of three diameters, are parallel to the load direction. The pile heads are hinged (zero bending moment) to the pile cap via appropriate kinematic constraints. The pile cap is considered axially incompressible so that the spacing among the pile heads is kept constant. Due to lack of space only results for the test P344 are presented herein.

The pile group is subjected to an asymmetric cyclic lateral loading similar to that of test P344 but with double amplitude (1920 kN). Fig. 20 plots the average force per pile versus group displacement and compares it with the corresponding force–displacement loop of the single isolated pile. For the same average load, the group displacement is greater than that of the solitary pile. Similar results have been derived by Rollins et al. [12] and Papadopoulou and Comodromos [22]. This behavior is attributed to that the passive failure zones of the piles in the group tend to overlap (shadow effect) as the lateral load increases, thus reducing the average soil resistance on the piles in the group. The shadow effect becomes more dominant with decreasing pile-to-pile distance. As in the case of the free-head single pile, the group displacement increases at a decreasing rate with the number of cycles finally reaching a plastic shakedown equilibrium. Interestingly, the force–displacement loop of the pile group is wider than the corresponding of the single isolated pile, implying greater soil plastification.

Figs. 21 and 22 depict the detailed distribution of the bending moments and the shear forces with depth along each pile in the group computed for different stages of loading. Comparison is given with the respective results from the analysis of the single isolated pile. The following observations are worthy of note:

- The maximum bending moment increases with the number of cycles and shifts to greater depths following the progressive extension of soil yielding. A similar trend in the behavior is exhibited by the shear force.
- The leading pile develops the largest bending moment in comparison to both the trailing and the single pile which shows an intermediate response. The discrepancy in the bending moment distribution between the trailing and the leading pile is attributed to the shadow effect. Similar trends are also observed in the shear force.
- Upon unloading, and for zero applied lateral force, the bending moments and shear forces are not zero. Instead, they retain large values comparable to those for the maximum applied load. Indeed, the reduction in the maximum values is about 40% for the bending moments and shear forces. It should be noted that in the case of a linear soil all the aforementioned quantities would vanish to zero, as soil elasticity would act as a restoring force for the pile.

The contours of the state parameter k are shown in Fig. 23. Evidently, the picture is similar to that of Fig. 10 for single pile response. The gradual expansion of the compression stress bulb with the number of cycles signals the plastic shakedown process until the pile group reaches a steady state equilibrium of constant plastic strain. The shadow effect is manifested by the formation of a relaxation zone ($k = 0$) at the back of the leading pile which softens the response of the trailing one.

Finally, Fig. 24 compares the efficiency factors for a 1 × 2 pile group loaded at a height 1.6 meters above the ground surface (should not be confused with pile-to-pile interaction factors) calculated with Model CT (complete modeling) and proposed by Reese and Van Impe [16]. It is interesting to observe, that the calculated efficiency factors converges to those of Reese and Van Impe [16] at very large pile head displacements, with a small discrepancy for the leading pile which shows to recover its initial stiffness

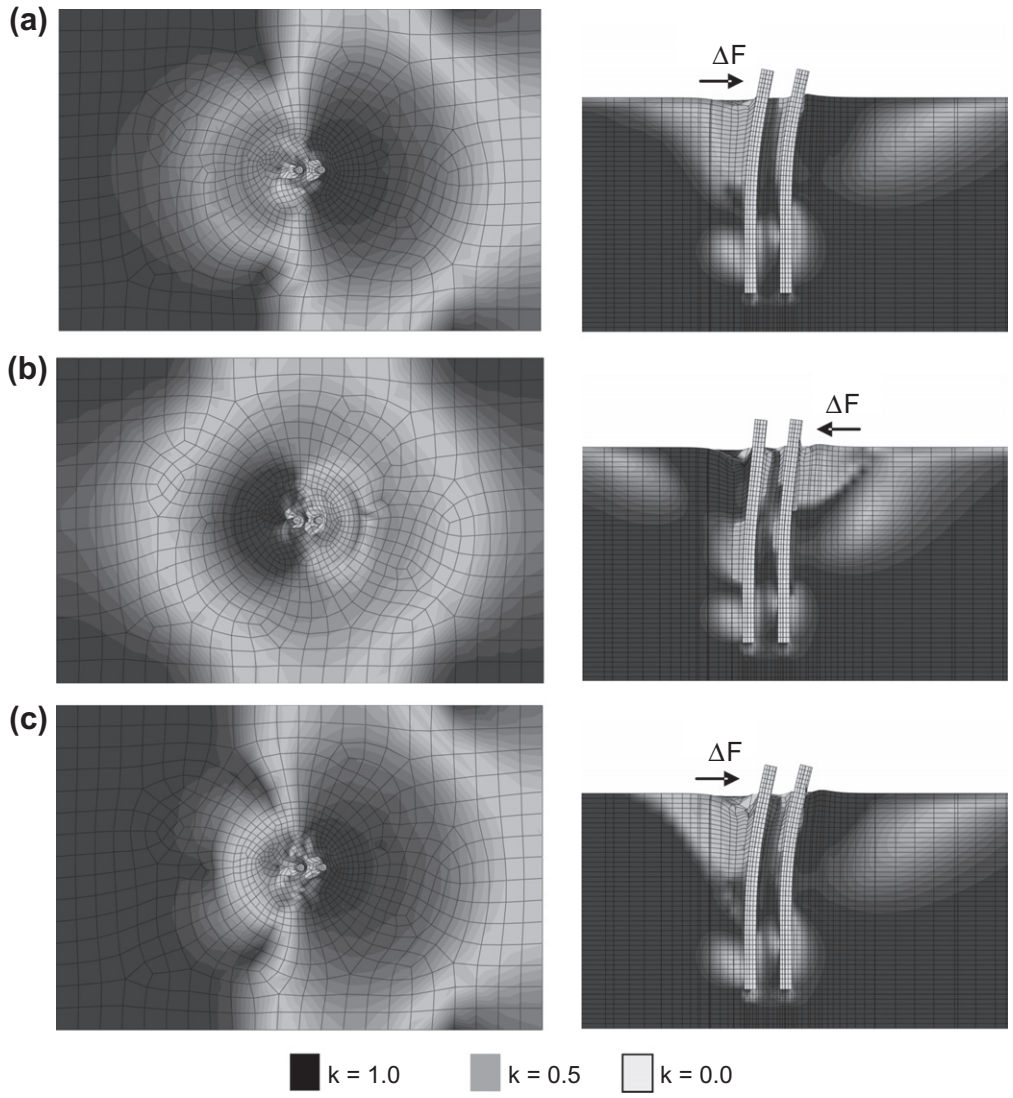

Fig. 23. Contours of the active and the passive stress states in terms of the state parameter k at three different stages of loading of the pile group: (a) at the 1st cycle at 960 kN, (b) at the 12th cycle at 0 kN, and (c) at the 12th cycle at 960 kN. $k = 1$ corresponds to pure triaxial compression loading condition (passive state), and $k = 0$ to pure triaxial extension loading condition (active state) while $k \approx 0.5$ sets the boundaries between the active and the passive state. (Deformation scale factor = 5.)

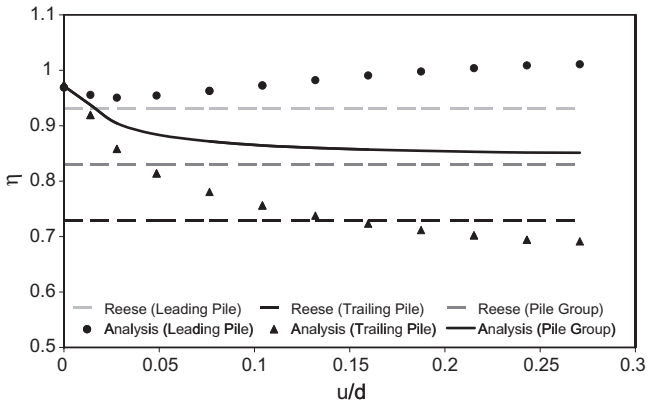

Fig. 24. Comparison of the calculated efficiency factors for a 1×2 pile group loaded at a height 1.6 meters above the ground surface with those proposed by Reese and Van Impe [16].

($\eta_L \approx 1$). A hardening response which may be attributed to the plastic shakedown effect. On the contrary, the computed efficiency factor for the trailing pile decreases with increasing horizontal displacement, as a result of the shadow effect, but at decreasing rate due the plastic shakedown induced hardening response of the pile group (reaching a minimum value of $\eta_t \approx 0.7$).

Of equal, if not more, interest is that at zero and/or very small pile displacements (elastic response), all the three computed efficiency factors (for the leading pile, the trailing pile and the pile group) are very close to 1 (≈0.97), implying that pile-to-pile interaction has an insignificant effect on the elastic response of the pile group. This could possibly suggest a "destructive" interference in pile-to-pile interaction rather than that pile-to-pile interaction factors are zero (which are certainly not, according to valid published results, e.g. Mylonakis and Gazetas [23]). It is recalled that the efficiency factor for a group of two piles, assuming elastic soil response and neglecting the cross-coupling (displacement/rotation atop the passive pile for a unit rotation/displacement atop the active pile) and rotational (rotation atop the passive pile for a unit rotation atop the active pile) pile-to-pile interaction factors, is expressed by:

$$\eta = \frac{1}{1 + \alpha_h} \tag{13}$$

in which α_h is the horizontal pile-to-pile interaction factor, approximated by [23]:

$$\alpha_h \approx \sqrt{\frac{d}{2s}} \tag{14}$$

with d the pile diameter, and s the pile-to-pile distance. For $d = 1$ m and $s = 3$ m, Eq. (13) yields $\eta = 0.71$ (compared to 0.97 in our analysis). Given that the rotational interaction factor is practically zero in our case, the comparison reveals the important role of the cross-coupling terms on the group efficiency.

The negligible pile-to-pile interaction effect is also evident in Fig. 20 which compares the computed force–displacement response of the single pile and the pile group.

7. Conclusions

A simplified constitutive soil model for the static and cyclic response of piles embedded in cohesionless soil was presented. Materialized into a three-dimensional finite element code, the model predictions were compared with experimental results of a single pile in dry sand, and subsequently the model was utilized in a numerical study. The numerical study addressed the cyclic lateral response of a group of two piles with similar geometric characteristics and soil conditions to those of the experimental tests. The main conclusions are:

- The plastic shakedown response of both the single pile and the pile group is mostly attributed to the so-called "system" densification rather than to cyclically-induced soil densification.
- Upon unloading to zero applied lateral force, the residual internal structural forces and the lateral soil reactions of the piles are substantial.
- The formation of a relaxation zone at the back of a leading pile (in the pile group) significantly reduces the lateral soil resistance on the trailing pile. This behavior, well-known in the literature as "shadow effect", is more prominent at large pile deformations.
- The efficiency factor of the leading pile decreases with increasing pile displacement but at extremely large deformations recovers if not overpasses its initial (near zero-amplitude-strain) value. On the contrary, the efficiency factor of the trailing pile decreases monotonically with loading, but at a decreasing rate, finally reaching an asymptotic value.
- The asymptotic values of all three efficiency factors (for the leading pile, the trailing pile and the pile group) compare well with those by Reese and Van Impe [16].
- Interestingly, and perhaps surprisingly, all the computed zero-amplitude strain efficiency factors are very close to 1, suggesting that pile-to-pile interaction effects are practically negligible. This stems mainly from the fact that the load is applied at a height above the soil surface, while the piles are hinged at their top.

Acknowledgements

The authors would like to acknowledge financial support from the EU 7th Framework research project funded through the European Research Council's Programme "Ideas", Support for Frontier Research – Advanced Grant, under Contract number ERC-2008-AdG 228254-DARE.

References

[1] Dawson TH. Simplified analysis of offshore piles under cyclic lateral loads. Ocean Eng 1980;7:553–62.
[2] Lin S, Liao J. Permanent strains of piles in sand due to cyclic lateral loads. J Geotech Geoenviron Eng 1999;125(9):798–802.
[3] Long JH, Vanneste G. Effects of cyclic lateral loads on piles in sand. J Geotech Eng 1994;120(1):33–42.
[4] Grashuis AJ, Dieterman HA, Zorn NF. Calculation of cyclic response of laterally loaded piles. Comput Geotech 1990;10:287–305.
[5] Hutchinson TC, Chai YH, Boulanger RW. Simulation of full-scale cyclic lateral load tests on piles. J Geotech Geoenviron Eng 2005;131(9):1172–5.
[6] Achmus M, Kuo Y, Abdel-Rahman K. Behavior of monopile foundations under cyclic lateral load. Comput Geotech 2009;36:725–35.
[7] Zhang F, Kimura M, Nakai T, Hoshikawa T. Mechanical behavior of pile foundations subjected to cyclic lateral loading up to the ultimate state. Soils Found 2000;40(5):1–17.
[8] Bourgeois E, Rakotonindriana MHJ, Le Kouby A, Mestat P, Serratrice JF. Three-dimensional numerical modeling of the behaviour of a pile subjected to cyclic lateral loading. Comput Geotech 2010;37:999–1007.
[9] Verdure L, Garnier J, Levacher D. Lateral cyclic loading of single piles in sand. Int J Phys Model Geotech 2003;3:17–28.
[10] Brown DA, Reese LC, O'Neill MW. Cyclic lateral loading of a large-scale pile group. J Geotech Eng 1987;113(11):1326–43.
[11] Tuladhar R, Maki T, Mutsuyoshi H. Cyclic behavior of laterally loaded concrete piles embedded into cohesive soil. Earthquake Eng Struct Dynam 2008;37:43–59.
[12] Rollins KM, Olsen RJ, Egbert JJ, Jensen DH, Olsen KG, Garrett BH. Pile spacing effects on lateral pile group behavior: load tests. J Geotech Geoenviron Eng 2006;132(10):1262–71.
[13] Poulos HG. Single pile response to cyclic lateral load. J Geotech Geoenviron Eng 1982;108:355–75.
[14] Rosquoët F, Garnier J, Thorel L, Canepa Y. Horizontal cyclic loading of piles installed in sand: study of the pile head displacement and maximum bending moment. In: Triantafyllidis T, editor. Proceedings of the international conference on cyclic behaviour of soils and liquefaction phenomena. Bochum: Taylor & Francis; 2004. p. 363–8.
[15] Garnier J. Properties of soil samples used in centrifuge models. In: Phillips R et al., editors. Invited keynote lecture, international conference on physical modelling in geotechnics – ICPMG '02, vol. 1. Rotterdam: A.A. Balkema; 2002. p. 5–19.
[16] Reese LC, Van Impe WF. Single piles and pile groups under lateral loading. Rotterdam: A.A. Balkema; 2001.
[17] Gerolymos N, Escoffier S, Gazetas G, Garnier J. Numerical modeling of centrifuge cyclic lateral pile load experiments. Earthquake Eng Eng Vib 2009;8:61–76.
[18] Gerolymos N, Gazetas G, Tazoh T. Static and dynamic response of yielding pile in nonlinear soil. In: Proceedings of the 1st Greece–Japan workshop: seismic design, observation and retrofit of foundations, Athens; 2005. p. 25–35.
[19] Gerolymos N, Gazetas G. Static and dynamic response of massive caisson foundations with soil and interface nonlinearities–validation and results. Soil Dynam Earthquake Eng 2006;26(5):377–94.
[20] Chen WF, Mizuno E. Nonlinear analysis in soil mechanics: theory and implementation. New York: Elsevier; 1990.
[21] Yang Z, Elgamal A. Multi-surface cyclic plasticity sand model with lode angle effect. Geotech Geol Eng 2008;26:335–48.
[22] Papadopoulou MC, Comodromos EM. On the response prediction of horizontally loaded fixed-head pile groups in sands. Comput Geotech 2010;37(7–8):930–41.
[23] Mylonakis G, Gazetas G. Vertical vibration and distress of piles and pile groups in layered soil. Soils Found 1998;38(1):1–14.